Performance of a Hybrid Catalyst from Amine Groups and Nickel Nanoparticles Immobilized on Lapindo Mud in Selective Production of Bio-hydrocarbons

Wega Trisunaryanti*, Salma Nur Azizah, Dyah Ayu Fatmawati, Triyono Triyono, and Novia Cahya Ningrum

Department of Chemistry, Faculty of Mathematics and Natural Sciences, Universitas Gadjah Mada, Sekip Utara, Yogyakarta 55281, Indonesia

* ***Corresponding author:***

email: wegats@ugm.ac.id

Received: November 23, 2021
Accepted: March 15, 2022

DOI: 10.22146/ijc.70667

Abstract: *In the present work, optimum conditions for hydrocracking of waste palm cooking oil (WPCO) over a Ni-NH_2/Lapindo mud catalyst were studied to obtain a high quantity and quality of biofuel. The utilized catalyst support material was Lapindo mud (LM) from Sidoarjo, Indonesia, which was only given physical treatment (i.e., washing, drying, grinding, and calcining). Ni/LM was prepared via wet impregnation in three different Ni weight loadings: 1, 5, and 10 wt.%, which were denoted as Ni(A)/LM, Ni(B)/LM, and Ni(C)/LM, respectively. As a result, the hydrocracking test of WPCO under the temperature of 470 °C and a feed/catalyst weight ratio of 50 showed that the Ni(A)/LM catalyst produced the highest liquid product reaching 46.65 wt.% among the other Ni-based catalysts. The liquid product can be increased drastically to 63.93 wt.% under a more optimum temperature at 550 °C. Functionalization of Ni(A)/LM as the best catalyst was carried out by grafting method with NH_2 groups from 3-APTMS, resulting in Ni(A)-NH_2/LM. This modification increased the liquid product to 68.17 wt.% under hydrocracking conditions using a weight ratio of 75. Moreover, the reusability of Ni(A)-NH_2/LM was found to be effective for three hydrocracking runs, constantly yielding an average biofuel of 80 wt.%.*

Keywords: *hydrocracking; Lapindo mud; nickel; 3-APTMS; waste palm cooking oil*

■ INTRODUCTION

The Lapindo mud (LM) flow disaster that occurred in 2006 in Porong, Sidoarjo, East Java, Indonesia, has not shown any improvement until now. One of the efforts to increase the use-value of LM is to convert it into a functional material. Based on research conducted by Kusumastuti et al. [1] stated that the LM consists of 49.24 wt.% Si, 19.30 wt.% Al, 14.06 wt.% Fe, and several elements in low quantities. This indicates that the LM is a potential source for the synthesis of silica-based materials. Among inorganic structures, silica (SiO_2) has been intensely studied for potential applications in catalysis, biological, biomedicine, etc., due to its abundance and simple synthesis method [2]. It is well-known that silica is intensively used in industry, indicating that it has low toxicity and is safe [3]. Some of the materials that have been successfully made using silica include Mobil Composition of Matter No. 41 (MCM-41), Santa Barbara Amorphous-15 (SBA-15), and mesoporous silica (MS). Mesoporous structures are characterized by having a large specific surface area and pores with diameters between 2 and 50 nm [4]. Mesoporous silica gained a raised interest, due to its extensive multi-functionality, based on its high specific surface area, uniform and tunable pore size, high pore volume, and facile functionalization [5]. Although mesoporous silica has advantages in terms of material characteristics and performance, synthesis methods involving many materials and complicated procedures limit its availability on an industrial scale [6]. Thus, we use the LM material directly as a natural catalyst support material without additional chemicals through easy initial preparation such as washing, drying, grinding, and calcining for removing volatile substances,

oxidizing a portion of the mass, or rendering them friable. This procedure has been done before by Trisunaryanti et al. [7], which utilizes beach sand with the main content of 43.09 wt.% Si, 12.91 wt.% Al, and 31.75 wt.% Fe as catalyst carrier materials. Although the material has a low specific surface area of 15.6 m^2/g, the overall catalyst is capable of producing 66.86 wt.% hydrocarbons, which is higher than using mesoporous silica as a catalyst carrier of 64.44 wt.%. This evidence allows that LM has tremendous potential as a catalyst support material as well as beach sand.

Supported nickel catalysts have attracted significant attention for their extensive applications in various industrial processes. During biomass conversion, nickel-based catalysts upgrade the composition of the liquid phase. Nickel metal has a relatively low price and a fairly high hydrogenation activity. In addition, the use of Ni metal as a catalyst can provide a high level of acidity from vacant p orbital [8]. This metal can increase catalytic activity and selectivity toward deoxygenated products [9]. The presence of incompleted orbitals in nickel metal can also play a good role in catalytic reactions and can homolytically break hydrogen gas in the hydrocracking process [1]. Jang et al. [10] have modified mesoporous silica with nickel-metal as a catalyst for hydrodeoxygenation and studied the effect of pore size and structure. The results of this study indicate that a high nickel content can reduce the surface area and pore volume of the silica support but does not affect the mesoporous structure. Paramesti et al. [11] have successfully tested the activity and selectivity of the Ni/MS catalyst against hydrocracking of waste cooking oil (WCO) into hydrocarbon compounds with variations in Ni concentration of 4%, 6%, and 8% (w/w). The results showed that the catalyst activity of Ni(4)/MS reached 80.57 wt.% and was more selective towards the formation of C_5-C_{12} chain hydrocarbon compounds of 54.22 wt.%.

The addition of the amine functional groups of 3-APTMS (3-Aminopropyltrimethoxysilane) to the surface of the silica support provides a Lewis base site derived from the electrons in the NH_2 groups [12]. This allows the groups to interact frequently with the acidic function in the feed compound, leading to more optimal free fatty acid (FFA) adsorption on the catalyst surface [13]. Interestingly, performing the reaction using a physical mixture of AP-MSN (AminoPropyl-Mesoporous Silica Nanoparticles) sorbent and Ni-MSN catalyst led to only 9 wt.% hydrocarbon yield compared to the 72 wt.% of hydrocarbons obtained using the hybrid AP-Ni-MSN as a catalyst [14]. The previous study also stated that the addition of amine groups to Ni-MS could increase the content of hydrocracking waste coconut oil from 47.7 to 68.8 wt.% and reduce FFA levels from 19.4 to 7.3 wt.%. This is due to the synergistic performance of the bifunctional adsorbent-catalytic nanoparticle material in converting FFA into hydrocarbons [8].

Today, the main energy source used in various countries is petroleum. Extensive and prolonged exploitation causes petroleum reserves to decrease. Among various refined petroleum products, gasoline and diesel are the fuels that are classified as the most widely used in transportation equipment [15]. Considering the importance of its use and availability, various efforts have been made to find alternative energy to replace these fuels. An alternative fuel that is currently very promising as a substitute for petroleum is palm oil [16]. But unfortunately, palm oil has the property of being easily oxidized because it contains fatty acids [17]. Direct use of palm oil can cause engine damage because the combustion products form deposits on the engine injector pipe and excess smoke [18]. In addition, palm oil also has a higher viscosity than petroleum [19]. From an economic point of view, direct use of palm oil is also less profitable because it will interfere with food security. Therefore, the conversion of waste palm cooking oil (WPCO) into biofuel is necessary so that it can be used as fuel without compromising food security. WPCO from the food industry and households is quite widely available in Indonesia. WPCO is harmful to health if reused for cooking because it contains a lot of FFA and radicals [20]. In addition, biofuels derived from vegetable oil are renewable fuels, easy to process, relatively stable in price, do not produce pollutants that are harmful to the environment (non-toxic), and are easily biodegradable [21].

The conversion of WPCO into biofuel is generally carried out through the hydrocracking method. This

method is a combination of thermal cracking and catalytic cracking involving the presence of hydrogen gas and catalyst material [22]. Activity, selectivity, stability, and product quality are the four keys to measuring the performance of hydrocracking catalysts [23]. Hydrocracking catalysts usually contain cracking sites from the support material such as silica, alumina, or zeolite, whereas hydrogenation sites are provided by the catalyst metal having d orbitals with unpaired electrons such as Pt, Pd, Co, Ni, Mo, etc. [24]. However, in this study, we involve the addition of amine groups that functions as an adsorption site of FFA in the feed so that the catalyst performance will be more optimal.

In this work, hydrocracking of WPCO will be carried out in the presence of a Ni-NH_2 catalyst prepared in LM as a support material. It is not only done to increase catalytic activity in producing hydrocarbon-based fuels but also on the use of natural sources to provide supporting materials with high availability and environmentally friendly. This LM will be used without any extraction process using chemicals that are harmful to the environment but only involve a simple physical process. Nickel metal deposited in the mud will be investigated through variations in loading weight where the most optimal loading weight in character and performance will be selected for functionalization using the amine groups of the 3-APTMS compound as represented in Fig. 1. The hydrocracking study on WPCO will be evaluated further through variations in the process temperature, feed/catalyst weight ratio, and reusability. Finally, the performance of each catalyst will be measured from the produced biofuel and their selectivity towards the gasoline and diesel fractions.

■ EXPERIMENTAL SECTION

Materials

The materials used in this study were Lapindo mud from Sidoarjo regency, East Java, Indonesia, as a source of catalyst support material, $NiCl_2{\cdot}6H_2O$ as Ni salt precursor (p.a) from Merck & Co, 3-APTMS (3-Aminopropyltrimethoxysilane, 97%) from Tokyo Chemical Industry, N_2 and H_2 gasses from PT. Samator Gas Industry, toluene (99.9%) and methanol (99.9%) from Merck & Co, distilled water, and waste palm cooking oil (WPCO) as feed in the hydrocracking reaction was collected from household waste.

Instrumentation

X-Ray Fluorescence spectrometer (XRF, analytical MiniPal 4) was used to determine the amount of metal/metal oxide in the material, X-Ray Diffractometer (XRD, Philips X'Pert MPD) was applied to identify the crystallinity of the material, Fourier-Transform Infrared Spectrometer (FT-IR, Shimadzu IRPrestige-21) was

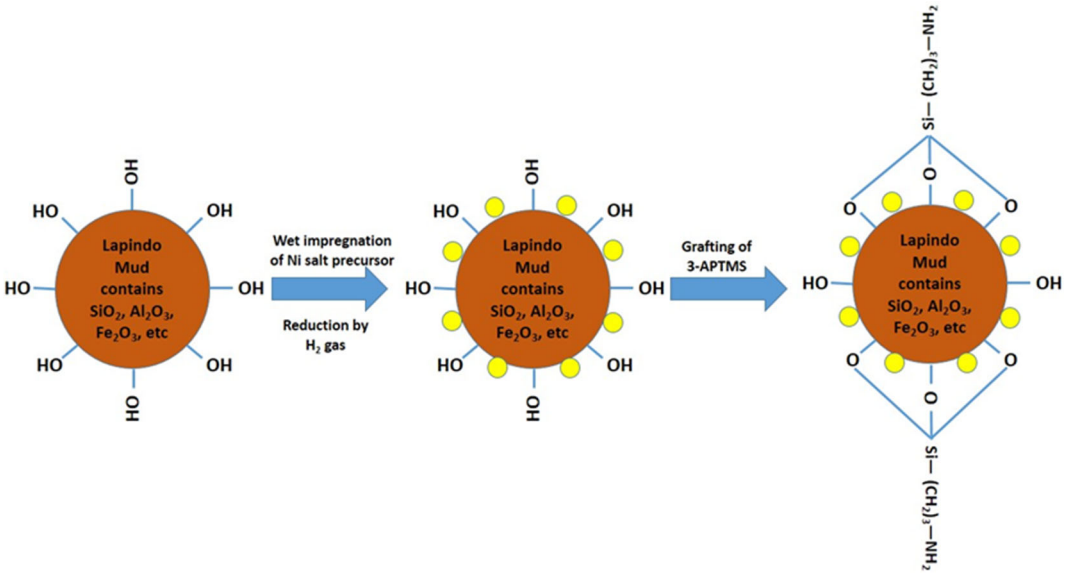

Fig 1. Diagrammatic representation of amine-grafted nickel/Lapindo mud material

utilized to analyze the characteristic functional groups in the material, Surface Area Analyzer (SAA, Quantachrome NOVAtouch 4LX) was used to observe the surface morphology of the material, and Transmission Electron Microscopy (JEOL JEM-1400 TEM) was utilized to characterize the nanostructure morphology of the material.

Procedure

Preparation of Lapindo mud as catalyst support material

First, Lapindo mud was washed with distilled water, then dried in an oven at 100 °C for 2 h. Next, the dried Lapindo mud was ground into fine particles until its size of 100 mesh. The sieved Lapindo mud was later called LM. After that, LM was calcined at a temperature of 500 °C, which is then called calcined Lapindo mud (CLM).

Preparation of Ni/Lapindo mud catalyst with various weight loadings of Ni metal

The nickel deposition process on the LM material was carried out by wet impregnation using $NiCl_2{\cdot}6H_2O$ as a salt precursor. First, 2 g of LM were put into a beaker and then suspended in 20 mL of distilled water. After that, Ni salt precursor with variations in Ni weight loading of 1, 5, and 10 wt.% to LM was added into the beaker. The mixture was stirred until homogeneous for 24 h at room temperature. The solution was directly evaporated and dried in an oven at 100 °C for 24 h. Afterward, the solid was calcined using N_2 gas at a flow rate of 20 mL/min at 500 °C for 3 h, followed by a reduction process using H_2 gas at the same condition to prepare zero valences of Ni metal. The resulting materials were then denoted as Ni(A)/LM, Ni(B)/LM, and Ni(C)/LM. Ni/LM catalyst with the highest total acidity value will be selected to be functionalized with NH_2 groups derived from 3-APTMS.

Functionalization of Ni/Lapindo mud with NH_2 groups originated from 3-APTMS

Modification of Ni/LM using 3-APTMS was carried out through the grafting method. Ni/LM was put into a flask and then injected with 3-APTMS until all surfaces became wet, then 20 mL of toluene was added. The mixture was refluxed for 6 h at 90 °C. The solids formed were separated from the solvent by centrifugation at 2000 rpm for 20 min. The sample was washed with methanol and then dried overnight at 80 °C.

Catalytic activity test through the hydrocracking process of waste palm cooking oil

Hydrocracking was applied by placing 0.1 g of each material as the catalyst and 5 g of waste palm cooking oil (WPCO) as feed in the column, then flowing hydrogen gas with a flow rate of 20 mL/min for 120 min at a temperature of 470 °C. The schematic illustration of the hydrocracking reactor can be seen in Fig. 2. The hydrocracking study was carried out through variations in process temperature, feed/catalyst weight ratio, and reusability test. The hydrocracking liquid product was then weighed to determine the activity of the catalyst. Meanwhile, Gas Chromatography-Mass Spectrometry (GC-MS, Shimadzu QP2010S) analysis was conducted to determine the selectivity of the catalyst to convert the feed into hydrocarbon compounds. The percentage conversion of hydrocracking products was estimated by the following calculations:

$$\text{Liquid (wt.\%)} = \frac{(\text{final flask weight} - \text{empty flask weight})}{\text{feed weight}} \times 100\% \quad (1)$$

$$\text{Coke (wt.\%)} = \frac{(\text{final catalyst container weight} - \text{initial catalyst container weight})}{\text{feed weight}} \times 100\% \quad (2)$$

$$\text{Residue (wt.\%)} = \frac{(\text{final feed container weight} - \text{empty container weight})}{\text{feed weight}} \times 100\% \quad (3)$$

$$\text{Gas (wt.\%)} = 100\% - (\text{Liquid} + \text{Coke} + \text{Residue}) \quad (4)$$

Based on the GC-MS analysis of the resulted hydrocracking liquid product, the selectivity of the catalyst was classified into four compound distributions, including gasoline (consisting of C_5-C_{12} chain hydrocarbon compounds), diesel (consisting of C_{13}-C_{20} chain hydrocarbon compounds), alcohol, and other oxygenates. The percentage of compound distributions in the liquid product can be determined by the following calculations:

$$\text{Gasoline (wt.\%)} = \frac{\text{GC area of C5} - \text{C12 compounds}}{\text{Total GC area}} \times \text{Liquid (wt.\%)} \quad (5)$$

$$\text{Diesel (wt.\%)} = \frac{\text{GC area of C13} - \text{C20 compounds}}{\text{Total GC area}} \times \text{Liquid (wt.\%)} \quad (6)$$

$$\text{Alcohol (wt.\%)} = \frac{\text{GC of alcohol compounds}}{\text{Total GC area}} \times \text{Liquid (wt.\%)} \quad (7)$$

$$\text{Others (wt.\%)} = \text{Liquid} - (\text{Gasoline} + \text{Diesel} + \text{Alcohol})\text{(wt.\%)} \quad (8)$$

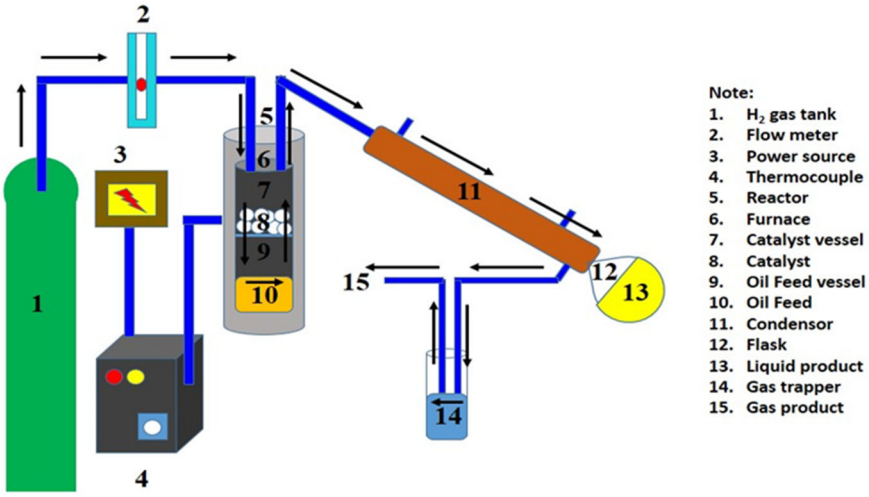

Fig 2. Schematic illustration of the hydrocracking reactor

■ RESULTS AND DISCUSSION

Catalysts Characterization

This research utilizes the catalyst carrier material in the form of mud from Porong, Sidoarjo. The XRF analysis results in Table 1 show the differences in the content of the main metal oxides between LM and CLM, namely silica, alumina, and iron oxides. According to Khoiri et al. [25], the silica and alumina contained in the mud can be used as catalyst support materials. From Table 1, it can be concluded that LM has more potential to be applied as a catalyst support material because it has a higher silica and alumina content than CLM. In addition, like other transition metals, the content of Fe_2O_3 also plays an important role in the hydrocracking process because the element Fe has a hydrogenation site as well as a Lewis acid site.

The impregnation of nickel-metal catalyst into the support material is carried out using the wet impregnation method with variations in the Ni weight loading on the LM support material by 1, 5, and 10 wt.%. The metal content itself plays an important role in the catalyst system because the presence of metal can contribute greatly to the Lewis acid site in the catalyst, where this active site affects the hydrocracking process. Based on the results of XRF analysis on the three catalysts, the nickel content of Ni(A)/LM, Ni(B)/LM, and Ni(C)/LM was 2.0, 6.9, and 17.5 wt.%, respectively. This difference in metal loading may be due to the oxidation state of Ni (x value) in the precursor salt $Ni(NO_3)_x{\cdot}6H_2O$ changes with storage time. Meanwhile, the calculation follows the x value listed on the packaging label.

Table 1. XRF analysis results on LM and CLM

Compound	wt.% content in LM	wt.% content in CLM
SiO_2	41.16	39.09
Fe_2O_3	18.24	19.24
Al_2O_3	12.84	12.22

The acidity test of the material was carried out using the gravimetric method, which compared the weight of the material before and after the adsorption of pyridine (C_5H_5N). This measurement is based on the amount of pyridine gas adsorbed by the material. Pyridine acts as a Lewis base having a lone pair of electrons on the N atom and as a Bronsted base accepting a proton to form a pyridinium ion ($C_5H_6N^+$).

Based on Table 2, it was found that the acidity of the mud decreased from 0.3533 to 0.2002 mmol/g after the calcination process. This is because the compounds that contribute to the acidity value are Al_2O_3, SiO_2, and Fe_2O_3. Looking back at the XRF results on the CLM, it revealed that the acidity value also decreased following the content of silica and alumina oxides. Here, because of the effect of high temperature on calcination, the iron oxide increases due to an increase in crystallinity. A 1% increase, on the other hand, indicates that the number has not changed considerably. This is the reason for choosing LM as a support material for the Ni catalyst in

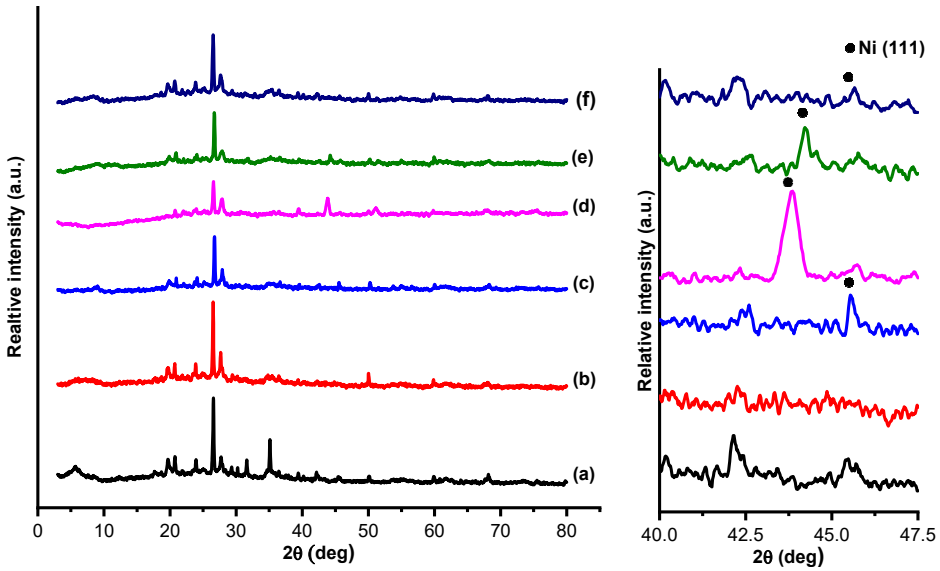

Fig 3. Diffractogram of (a) LM, (b) CLM, (c) Ni(A)/LM, (d) Ni(B)/LM, (e) Ni(C)/LM, (f) Ni(A)-NH_2/LM

Table 2. Acidity value of the materials

Material	Acidity (mmol/g)
LM	0.3533
CLM	0.2002
Ni(A)/LM	0.4087
Ni(B)/LM	0.0758
Ni(C)/LM	0.1517
Ni(A)-NH_2/LM	0.2289

Notes: acidity test was gravimetrically done to calculate the acid sites in the material using pyridine as a base adsorbate

the wet impregnation process.

The acidity test on this catalyst aims to see the contribution of the presence of nickel-metal that has been deposited on the LM material. Nickel metal is a transition metal group with an empty 4p electron orbital where this orbital acts as a Lewis acid site. Therefore, the presence of Lewis acid sites is expected to increase the acidity of the catalyst. Based on Table 2, Ni(A)/LM catalyst has the highest acidity compared to Ni(B)/LM and Ni(C)/LM catalysts. In fact, this is contrary to the theory that acidity increases with metal content. However, in another theory, the low metal content tends to make the nanoparticles evenly distributed on the surface of the supporting material. The non-closure of pores by nanoparticles also results in more optimal pyridine adsorption so that the acidity increases. According to Nugrahaningtya et al. [26], the presence of an increasing amount of metal loading makes the pores in the carrier material unable to adsorb due to steric resistance. In addition, an increase in Ni metal can cover the catalyst cavity, causing the Lewis acid site to be closed due to agglomeration. The agglomeration that occurs makes the acidity of the catalyst decrease, as happened in the Ni(B)/LM and Ni(C)/LM catalysts. But in this case, the higher acidity of catalyst Ni(C)/LM than Ni(B)/LM implies that the theory of the amount of metal content is stronger than the theory of metal distribution. Based on the acidity values of the three catalysts, Ni(A)/LM was chosen as the material to be grafted by the NH_2 groups of 3-APTMS. Meanwhile, after the acidity test was carried out on the material, the Ni(A)-NH_2/LM catalyst had a lower acidity than Ni(A)/LM. This is due to the presence of aminopropyl groups, which tend to be base.

XRD analysis was performed to evaluate the crystallinity character of the material. The type of compound or element can be seen from the peak that appears at the diffraction angle (2θ), while the crystallinity level of the catalyst can be seen from the peak intensity. The compilation of the diffractogram in Fig. 3 shows that all types of materials produce crystal peaks in the 2θ region between 20° to 40°. Similar results were obtained from other studies conducted by Kefaifi et al. [27]. In their research, it was revealed that these peaks are characteristic peaks of the element silicon in

the form of SiO_2 minerals. Meanwhile, the diffractogram of this study shows 2θ at 26.59° with an intensity of 100%, which is a type of quartz mineral SiO_2 with d-spacing 101 = 3.35 nm based on ICDD data 01-083-0539. In addition, the presence of alumina in the form of $AlPO_4$ (aluminum phosphate) in XRD spectra is shown at the peak of 2θ = 26.49°, which has an intensity of 100% with d-spacing 012 = 3.36 nm based on data on ICDD 01-084-0853. These peaks do not appear in the spectra because they are in a region similar to silica which allows overlapping. However, the presence of alumina compounds has been identified in the XRF data as well as silica.

Based on Fig. 3, it can be seen that after calcination, most of the crystalline peaks in LM experienced a decrease in intensity, as seen in the CLM, Ni(A)/LM, Ni(B)/LM, Ni(C)/LM, and Ni(A)-NH_2/LM spectra. In addition, the peak at 36.48° of the 110 crystal plane (based on data on ICDD 01-083-0539) in the LM disappeared after calcination. This is because the calcination process aims to form oxide compounds, rearrange the content of compounds in the material, and evaporate volatile compounds that can affect the structure of the material.

The presence of nickel-metal character in the diffractograms is indicated by crystal peaks that appear at 2θ of around 43–45° based on JCPDS no. 02-0850. The size of the Ni crystallite in the catalyst material can be calculated using the Scherrer equation as follows:

$$D = \frac{0.9\lambda}{\beta \cos\theta}$$

where D is the crystal size in nanoparticles (nm), β is full width at half maximum (FWHM, radian), θ is Braggs angle (radian), and λ is X-ray wavelength (λ = 1.54 nm for Cu Kα radiation). According to the equation, it is formulated that FWHM is inversely proportional to the crystallite size (D), so larger peaks result in smaller crystallite sizes. From the calculation results, the crystallite sizes for Ni(A)/LM, Ni(B)/LM, and Ni(C)/LM catalysts were 57.17, 18.15, and 33.65 nm, respectively. Meanwhile, the Ni(A)-NH_2/LM catalyst has a nickel crystallite size of 48.04 nm. This value is similar to that of the Ni(A)/LM catalyst, which indicates that the NH_2 grafting of 3-APTMS does not affect the crystallinity properties of the Ni(A)/LM catalyst. The large crystallite size is possible from a combination of smaller nanoparticles that agglomerate to form larger nanoparticles. Furthermore, although there is a trend, agglomeration is not always associated with high metal content. Agglomeration causes the nanoparticles to be unevenly distributed to the surface of the supporting material.

FTIR characterization aims to determine the presence of characteristic functional groups of material. Based on the results of the FTIR analysis in Fig. 4, it can be seen that there are characters of silica-alumina groups in all materials, which confirms the previous XRF and XRD results. These groups are represented by the symbol T as shown in Table 3. The presence of silica-alumina groups indicates that LM has the potential to be used as a catalyst carrier material. In addition, there is a left shift of the absorption peak in the T–O–T asymmetric stretching vibration in the CLM. This indicates the occurrence of dehydration on the surface of the silica-alumina, which makes the water release leaving alumina ions and then forming Lewis acid sites in the non-framework. Similar results also occurred in the study conducted by Dubey et al. [28]; there was a shift in the absorption peak from 1065 to 1080 cm^{-1} in MCM-41 before and after calcination. Meanwhile, the variation in the weight loading of the Ni on the LM did not significantly affect the vibration absorption produced. After the NH_2 grafting process on Ni(A)/LM

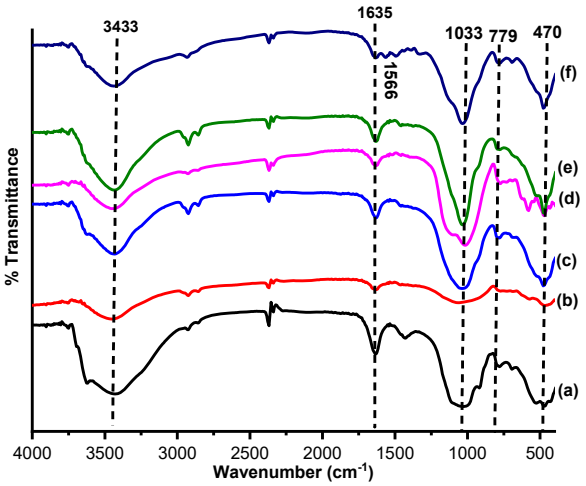

Fig 4. FTIR spectra of (a) LM, (b) CLM, (c) Ni(A)/LM, (d) Ni(B)/LM, (e) Ni(C)/LM, (f) Ni(A)-NH_2/LM

was carried out, a new characteristic functional group has emerged with low intensity namely $-NH_2$ at 1566 cm^{-1} derived from the 3-APTMS compound. This modification process was successful because there was a decrease in the intensity of the T–OH bending vibration due to the interaction between T–OH and 3-APTMS. These results are under the research conducted by Li et al. [29].

The nitrogen adsorption isotherm for the synthesized material is presented in Fig. 5. Several materials (except Ni(A)-NH_2/LM) exhibited a type IV isotherm corresponding to the characteristics of the mesoporous material, according to the IUPAC classification. This graph shows that metal impregnation does not damage the mesoporous properties of the support material. The process that occurs in this type of isotherm starts from adsorption at low pressure (< 0.02) for micropore filling, followed by monolayer and multilayer adsorption on the surface of the material, including mesopores, at medium relative pressure (0.2–0.5) the phenomenon of capillary condensation occurs in the mesopores. At this point, the amount of adsorbed gas increases sharply with a small pressure change due to the condensation of the molecules under the vapor

Table 3. Analysis result of FTIR spectra

Vibration type	Wavenumber (cm^{-1})					
	LM	CLM	Ni(A)/LM	Ni(B)/LM	Ni(C)/LM	Ni(A)-NH_2/LM
Bending of T–OH	1635	1635	1635	1635	1627	1635
Stretching of T–OH	3425	3448	3433	3448	3433	3433
Asymmetric stretching of T–O–T	1033	1064	1033	1018	1033	1033
Symmetric stretching of T–O–T	779	725	779	771	779	779
Bending of T–O–T	470	462	478	470	470	478
Bending of -NH_2	-	-	-	-	-	1566
Stretching of C–H	2924	2924	2924	2924	2924	2931

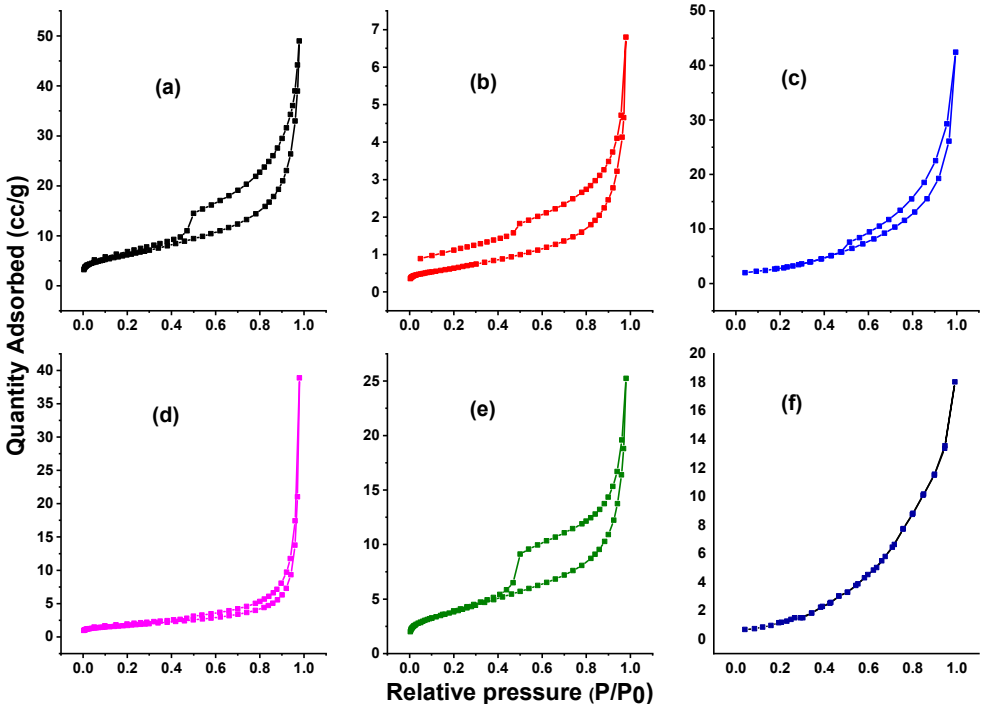

Fig 5. Nitrogen adsorption-desorption isotherm of (a) LM, (b) CLM, (c) Ni(A)/LM, (d) Ni(B)/LM, (e) Ni(C)/LM, (f) Ni(A)-NH_2/LM

pressure so that the liquid adsorbate fills the primary mesoporous. Thereafter, multilayer adsorption and/or condensation of liquids in the secondary mesopores occur at relatively high pressures (0.5–0.8) and finally at very high pressures (< 0.8), corresponding to the filling of voids between particles which can be considered as porosity [30]. The Ni(A)-NH_2/LM material shows a different type of isotherm from other materials. This material belongs to the type III category where there is no identifiable multilayer formation, meaning that there are relatively weak adsorbent–adsorbate interactions [31].

This typical mesoporous material is represented by the presence of a hysteresis loop at the isotherm. The type of hysteresis possessed by these materials follows the H3 pattern as described by IUPAC, where the desorption branch tends to be perpendicular to the adsorption branch in the closure region at lower relative pressures. In the hysteresis loop H3, the pores have a wedge or slit geometry, resulting from agglomerates of parallel plates-shaped particles [32]. The hysteresis loops never close in all these materials, even under very low pressure, as happened to CLM. This can be attributed to several reasons. First, the material is not a rigid structure and may deform, induced by adsorption or pore filling. Second, the trapped nitrogen cannot be released because of the affinity of nitrogen in the material caused by the heterogeneous property of the surface [33]; the adsorption potential of the pore wall traps the nitrogen molecules, which agrees with the observation that increasing temperature will deteriorate the hysteresis effect [34].

The pore distribution of the materials can be seen in Fig. 6. All pores in the material belong to the mesoporous class, where the diameter is between 2–50 nm. The pore diameter is taken from the highest point on each bar chart, representing the most frequent pore diameter based on the BJH desorption method. Meanwhile, the material surface area is calculated using the BET method. There was a drastic decrease in the surface area of LM after calcination from 22 to 2 m^2/g. This is because the silica and alumina content in LM decreases during the heating process [35], which is in line with the decrease in acidity value. Another decrease also occurred in LM loaded with Ni metal, where the surface area decreased following the increasing weight of metal loading. Among Ni catalysts, the smallest surface

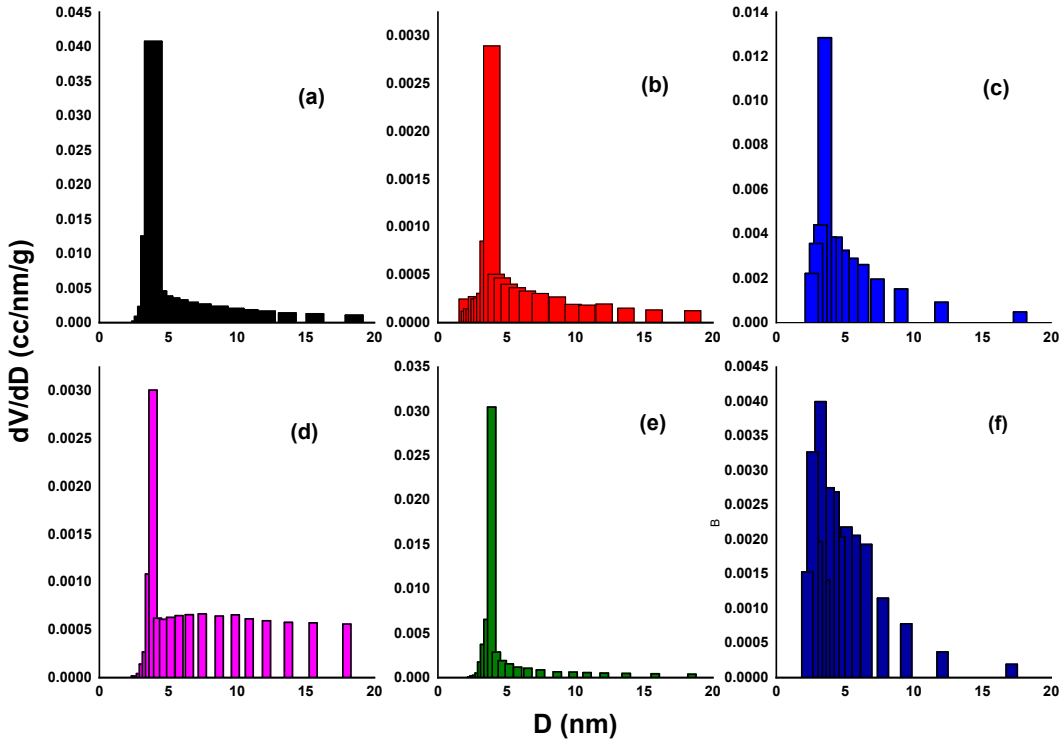

Fig 6. Pore size distribution of (a) LM, (b) CLM, (c) Ni(A)/LM, (d) Ni(B)/LM, (e) Ni(C)/LM, (f) Ni(A)-NH_2/LM

area is owned by Ni(B)/LM, which is possible due to the blockage of the pores of the material, strengthened by the lowest acidity value. The presence of 3-APTMS modification also contributed to the decrease in the surface area of Ni(A)/LM. Overall, the surface area of the material obtained is quite small, which is below 25 m^2/g. In theory, the high metal content and small particle size lead to a large surface area. This situation can be achieved if the nanoparticles are evenly distributed and do not block the pores of the supporting material [36]. The large nanoparticle size also contributes to the increase in surface area, although not as much as the small nanoparticles. However, in this case, we can only measure the metal content, but not the degree of distribution and pore-clogging. Data analysis of the textural properties of the material is presented in Table 4.

Study of Catalytic Activity and Selectivity

To evaluate the catalytic activity, all prepared catalysts were applied for the hydrocracking process of waste palm cooking oil (WPCO) at a temperature of 470 °C with a feed:catalyst weight ratio of 50. The catalyst that generates a liquid product with the highest level of hydrocarbons would be considered as the best catalyst and will be studied further to find the optimum conditions for the hydrocracking process.

The results of all the hydrocracking that have been shown by each catalyst are summarized in Table 5. Interestingly, the LM support material in the absence of Ni gave an excellent performance with a total liquid product of 56.30 wt.%. This provides a new point of view that natural material without chemical treatment has good catalytic activity, although its surface area is small (22.216 m^2/g) compared to other supports. Here, the calcination process in CLM shows its role in increasing the total liquid product up to 66.71 wt.%. As previously described, this process has several functions, including removing impurities. However, because of its low acidity value from the content of silica oxide and alumina as the main constituents, this material (31.1 wt.%) resulted in the hydrocarbon content being lower than LM (55.20 wt.%). Several reasons (high acidity, large surface area, and high hydrocarbon product) made LM chosen as a support material for Ni catalysts through a wet impregnation process.

Generally, the hydrocracking process consists of two

Table 4. Textural properties of materials

Material	Surface area (m^2/g) [a)]	Most frequent pore diameter (nm) [b)]	Total pore volume (cc/g) [c)]
LM	22.216	3.916	0.060
CLM	2.304	3.908	0.007
Ni(A)/LM	11.659	3.528	0.062
Ni(B)/LM	6.155	3.906	0.033
Ni(C)/LM	13.797	3.906	0.029
Ni(A)-NH_2/LM	5.953	3.225	0.028

Notes: [a)] based on BET calculation
[b)] based on BJH Desorption
[c)] at $P/P_0 = 0.99$

Table 5. Distribution of hydrocracking products based on the type of catalyst

Catalyst	Liquid (wt.%)					Gas (wt.%)	Coke (wt.%)	Residue (wt.%)
	Gasoline	Diesel	Alcohol	Others	Total			
LM	38.14	12.08	3.03	3.05	56.30	41.06	1.35	1.29
CLM	23.91	7.19	20.36	15.25	66.71	30.50	0.29	2.50
Ni(A)/LM	39.89	1.81	1.15	3.80	46.65	47.59	3.73	2.03
Ni(B)/LM	40.94	0.00	0.38	1.51	42.83	55.58	0.41	1.18
Ni(C)/LM	18.83	13.26	3.69	4.60	40.38	58.58	0.04	1.00

Notes: Temperature of 470 °C, feed/catalyst weight ratio of 50

reactions, namely hydrogenation and cracking. Hydrogenation involving the presence of hydrogen gas provides a role for further deoxygenation reactions, namely decarbonylation, decarboxylation, and hydrodeoxygenation. Both decarbonylation and decarboxylation release one C atom in the form of CO and CO_2, producing a hydrocarbon with one fewer carbon atom [2]. Meanwhile, hydrodeoxygenation only releases O atoms in the form of H_2O through a consecutive reduction process so that the hydrocarbon has a carbon length identical to the initial oxygenated compound as happened with CLM, which produces high alcohol products as a result of the final consecutive reduction.

In this case, all the catalysts used gave selectivity to the gasoline product, indicating that the deoxygenation reaction occurred to produce heavier hydrocarbons before being taken over by the cracking reaction to produce lighter hydrocarbons. With the advent of solar products, the reaction may stop only on deoxygenation. Ochoa-Hernández et al. [37] stated that an increase in acidity from Ni would cause the hydrotreatment process to run non-selectively towards the production of long-chain hydrocarbons through hydrodeoxygenation and decarboxylation. The addition of Ni makes the active site on the catalyst increase so that the catalyst becomes super active, which results in secondary cracking. Among the three Ni-based catalysts (Fig. 7), the Ni(A)/LM material provided the highest level of hydrocarbons (41.7 wt.%). This confirms that the acidity value is correlated with the hydrocarbon level. The higher diesel product at Ni(C)/LM compared to others is possible due to the blockage of the pores from agglomeration or deposition of the metal nanoparticles, causing a decrease in the number of accessible acid sites for the feed molecules. This pushes the deoxygenation reaction mechanism predominantly to produce heavier hydrocarbons and causes the splitting of larger molecules to become smaller in the cracking mechanism to be inhibited [38]. When compared with all the tested materials, LM produced the highest hydrocarbon products even without the addition of Ni metal. However, the aim of this study was not only to find the best catalyst in hydrocracking activity and selectivity but also to study the development of catalyst materials, in this case, LM as a natural-based catalyst support material without prior chemical treatment.

Despite producing good performance with a total liquid product and hydrocarbon content reaching 46.65 and 41.70 wt.%, the catalytic activity of the WPCO hydrocracking process using a Ni(A)/LM catalyst can still be improved by selecting the best temperature. This variation is carried out and observed to find the best conditions. As shown in Table 6, the highest conversion was obtained in hydrocracking at a temperature of 550 °C. At this temperature, the conversion level of WPCO increased to 63.93 wt.% compared to temperatures of 470 °C (46.65 wt.%) and 500 °C (53.09 wt.%). The increase in temperature may provide more energy in the system which will promote the adsorption force of the feed on the catalyst surface, causing the reaction rate to increase. According to Murachman et al. [22], the reaction rate constant is a function of temperature. This is because the

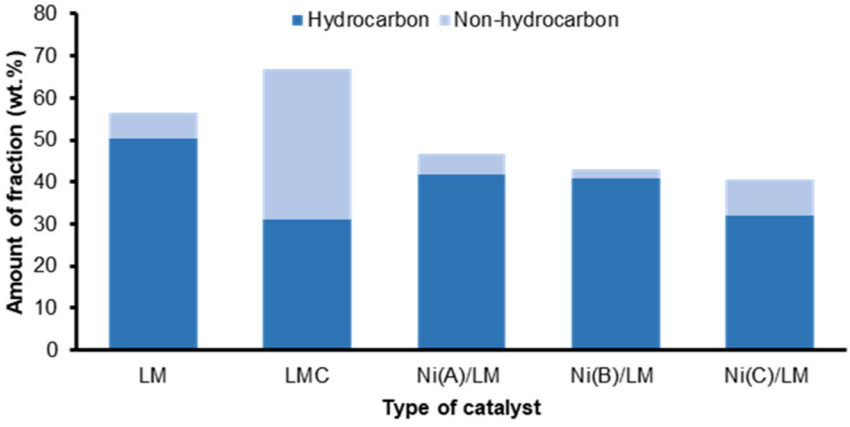

Fig 7. Effect of catalyst type on hydrocarbon and non-hydrocarbon

Table 6. Distribution of hydrocracking products based on various temperatures

Temperature (°C)	Liquid (wt.%)					Gas (wt.%)	Coke (wt.%)	Residue (wt.%)
	Gasoline	Diesel	Alcohol	Others	Total			
470	39.89	1.81	1.15	3.80	46.65	47.59	3.73	2.03
500	26.01	11.24	6.70	9.14	53.09	41.72	4.57	0.62
550	30.81	5.27	19.14	8.71	63.93	30.67	4.98	0.42

Notes: Ni(A)/LM catalyst, feed/catalyst ratio weight of 50

chance of collisions between molecules is getting bigger, which makes the average kinetic energy of the molecules increase. Not to mention, the optimum temperature also reduces feed residue to 0.42 wt.%.

As the previous results, in this condition, all temperatures provide selectivity for gasoline products (Fig. 8). Although 550 °C produces lower levels of hydrocarbons (36.08 wt.%) than at 500 °C (37.25 wt.%) and 470 °C (41.70 wt.%), its activity (amount of liquid product) shows the best performance. Moreover, it can be seen that this temperature gives a very high alcohol content of 19.14 wt.%. If it can be separated, this alcohol also provides benefits as a fuel mixture to increase the octane number [39]. A high octane number makes fuel efficiency increase so that it can cover its low energy density (when compared to gasoline or diesel), but the maximum content is only 10%. The presence of alcohol as a by-product suggests that this reaction mechanism follows hydrodeoxygenation which results in a step-by-step reduction of the carboxyl to aldehyde and ends to the alcohol. The decrease in selectivity is possible because the adsorption rate is too fast at high temperatures resulting in a less optimal reaction for converting oxygenated compounds into hydrocarbons.

In addition to Ni, secondary cracking also occurs because the catalyst support used is LM which naturally contains high levels of iron oxide. This Fe metal also provides Lewis acid sites which cause the catalyst to be super active so that the cracking becomes uncontrolled, causing the liquid phase produced to turn into a gas phase. The high gas product indicates that this process favors the production of the lightest hydrocarbon molecules due to the cleavage of the C–C or C–H bonds in the alkyl triglyceride or FFA chains.

In addition to the optimum temperature, the feed/catalyst weight ratio in hydrocracking also needs to be further investigated to obtain the best conditions to produce biofuels with high hydrocarbon content. In this study, a Ni(A)-NH_2/LM catalyst was also involved in determining the role of the NH_2 groups of the 3-APTMS compound on the surface of the LM. Based on Table 7, it can be seen that there is an increase in the conversion of Ni(A)/LM along with the weight ratio. However, the hydrocarbon selectivity decreased to only 4.47 wt.% at a ratio of 100. The grafting treatment on Ni(A)-NH_2/LM provided the Lewis base site from the lone pair of the nitrogen atom [40]. This makes the catalyst easier to capture and adsorb FFA in the feed, resulting in a higher

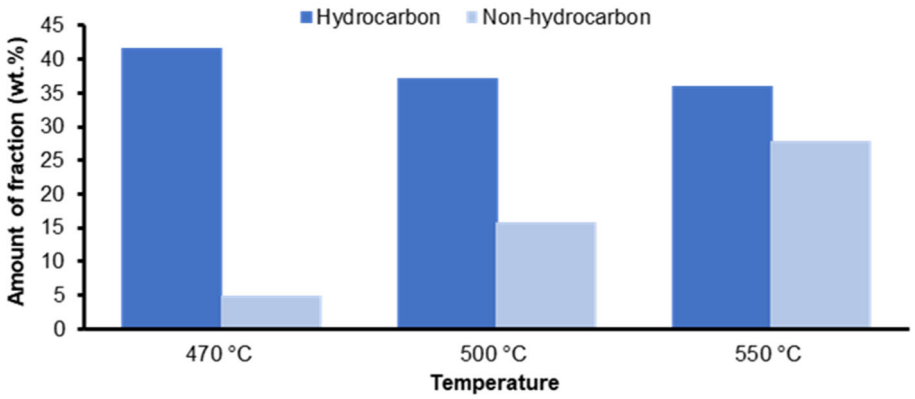

Fig 8. Effect of hydrocracking temperature on hydrocarbon and non-hydrocarbon

Table 7. Distribution of hydrocracking products based on a feed/catalyst weight ratio

Catalyst	Ratio	Liquid (wt.%)					Gas (wt.%)	Coke (wt.%)	Residue (wt.%)
		Gasoline	Diesel	Alcohol	Others	Total			
Ni(A)/LM	50	30.81	5.27	19.14	8.71	63.93	30.67	4.98	0.42
	75	12.99	18.14	29.77	7.12	68.02	26.36	2.96	2.66
	100	2.10	2.37	65.28	7.81	77.56	17.87	2.60	1.97
Ni(A)-NH_2/LM	50	26.91	4.31	16.11	17.70	65.03	32.81	1.17	0.99
	75	17.20	16.72	25.44	8.81	68.17	29.08	0.69	2.06
	100	8.03	9.56	28.21	4.04	49.84	48.73	0.94	0.49

Notes: Temperature of 550 °C

conversion than Ni(A)/LM at the same ratio. Although, in fact, at a ratio of 100, there was a decrease in biofuel up to 49.84 wt.%, possibly because too much feed was used, so the amount of catalyst could not accommodate the reaction optimally. The higher amount of feed will naturally enter the catalyst pores, inhibiting and slowing the feed flow, leaving a higher residue level. The presence of residue indicates that this process requires a longer reaction time. It could also be occurred due to polymerization to form heavier and larger molecules, which accumulate as residues. Pore filling during hydrocracking also results in carbon trapping, increasing overall coke deposition.

The synergistic action between Ni nanoparticles and NH_2 groups provides good catalyst selectivity toward hydrocarbon products. Meanwhile, the results at a ratio of 50 showed a 4.86% decrease in the hydrocarbon content from Ni(A) to Ni(A)-NH_2, which was possible under these conditions that were unfavorable for the catalyst. However, when viewed from the economic side, by using more feed oil (the ratio is higher), the catalyst containing NH_2 has better results. According to Fig. 9, the optimum ratio in converting WPCO to hydrocarbons (33.92 wt.%) using a Ni(A)-NH_2/LM catalyst is 75. The combination of NH_2 groups, acid sites, and hydrogenation sites causes this interaction to weaken the CO or C=O bonds, then intensifies the deoxygenation mechanism to produce hydrocarbons.

The use of Ni(A)-NH_2/LM catalyst is tested for durability after reuse, which is known as the catalyst reusability test. The age test was carried out using the same catalyst without being replaced and given any treatment after use. The reusability of Ni(A)-NH_2/LM in 3 runs of WPCO hydrocracking at 550 °C using a ratio of 75 was studied (Table 8). Interestingly, during these 3 runs, the catalyst was shown to produce an astonishing

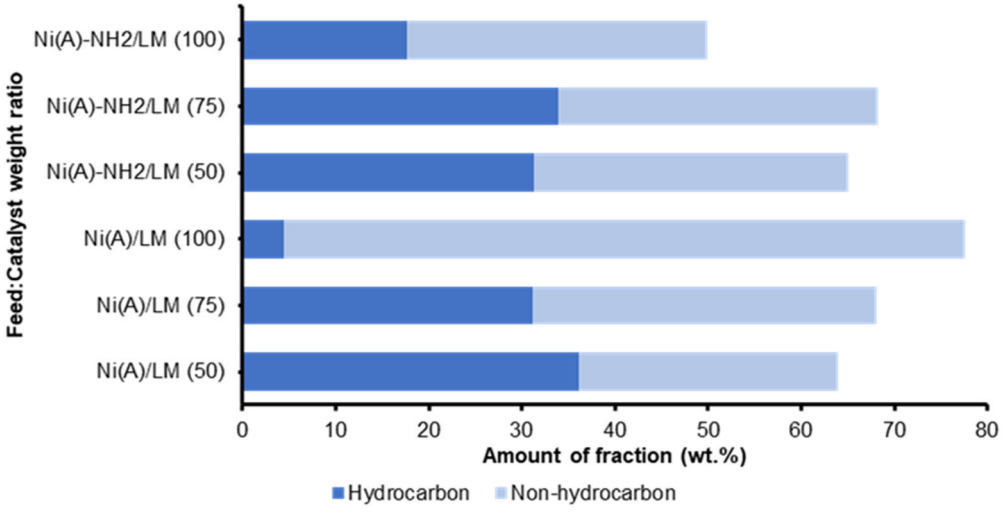

Fig 9. Effect of feed/catalyst weight ratio on hydrocarbon and non-hydrocarbon

result with a consistently high conversion level (~80 wt.%). The formation of coke is also seen to relatively occur at a controlled rate, indicating stability towards coke poisoning.

Despite the total liquid product increases, not all of the constituent compounds of this liquid product can be used as fuel. Selectivity studies cannot be carried out by looking at the percentage of liquid products because the trend always increases without showing a significant decrease. Therefore, this study will focus on the ability of the catalyst to direct the hydrocracking reaction to produce hydrocarbon products. Fig. 10 shows that the hydrocarbon level decreased drastically with the frequent use of the catalyst. This indicates that the active sites of catalysts such as NH_2 groups and Ni nanoparticles have started to decrease in performance due to repeated use. However, until the third use, the amount of hydrocarbons is still relatively high at 38.36 wt.%. This gives the view that this catalyst can still show good performance so that it can be used more than 3 times.

TEM analysis aims to see the morphology, structure, and pore regularity. The results of the TEM image presented in Fig. 11 imply the catalyst that has been used in the hydrocracking process experiences a

Table 8. Distribution of hydrocracking products based on reusability

Use	Liquid (wt.%)					Gas	Coke	Residue
	Gasoline	Diesel	Alcohol	Others	Total	(wt.%)	(wt.%)	(wt.%)
1	49.28	12.56	5.47	12.15	79.46	20.29	0	0.25
2	32.63	8.42	8.05	31.17	80.27	19.49	0	0.24
3	28.73	9.63	23.66	22.31	84.33	15.13	0	0.54

Notes: Ni(A)-NH_2/LM catalyst, Temperature of 550 °C, feed/catalyst ratio weight of 75

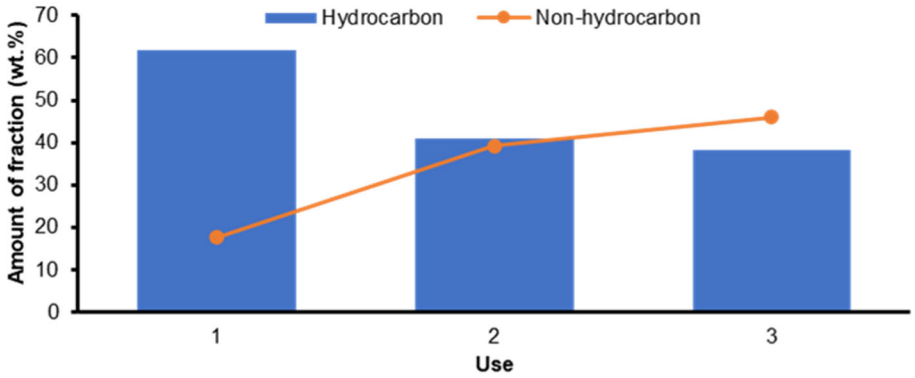

Fig 10. Effect of reusability on hydrocarbon and non-hydrocarbon products

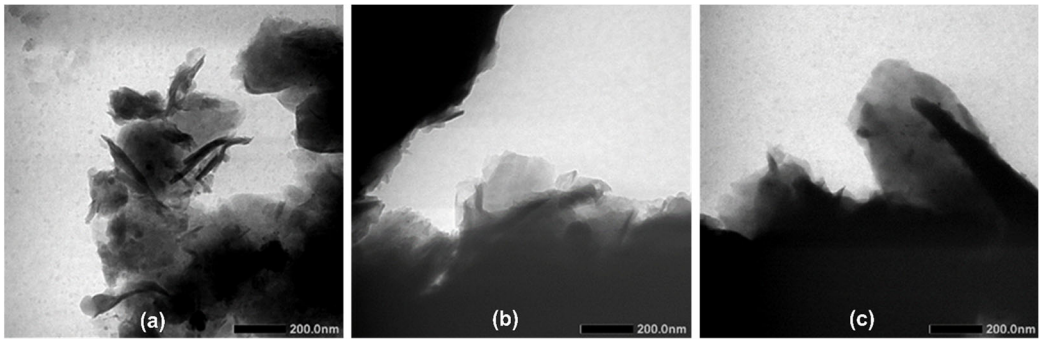

Fig 11. TEM images of (a) Ni(A)-NH_2/LM (75) before hydrocracking, (b) Ni(A)-NH_2/LM (75) after hydrocracking, (c) Ni(A)-NH_2/LM (100) after hydrocracking

darker color change due to the formation of coke deposition. The Ni(A)-NH_2/LM catalyst with a feed/catalyst ratio of 100 (Fig. 11(c)) looks very dark compared to Fig. 11(b), which explains that the pores of the catalyst have been closed due to the high interaction with the feed. This is evident from the coke production presented in Table 7 previously.

■ CONCLUSION

The hydrocracking study of waste palm cooking oil (WPCO) was prepared using natural catalyst support materials from Lapindo mud (LM), Sidoarjo, Indonesia, without any chemical treatment. This material is proven to have a high content of silica, alumina, and iron oxides. Even without the calcination process, this material has a higher acidity value which makes it effective as a Ni carrier. The weight of Ni loading on the LM at 1 wt.% gave the highest acidity value compared to 5 and 10 wt.%, following the obtained biofuel. This proves that a high weight loading does not always give a high catalytic activity as well because behavior like an agglomeration of the catalyst covering the support pores sometimes occurs in this situation. Interestingly, the small specific surface area of LM is capable of producing a high biofuel level of 56.30 wt.% with a hydrocarbon content of 50.22 wt.%. Process temperature and the weight ratio of feed/catalyst also affect the hydrocracking reaction. High temperatures will increase the reaction rate so that the kinetic energy between particles is getting bigger, causing more liquid products to be generated. Meanwhile, the obtained optimum ratio is at 75, where this ratio is increased more, the work of the catalyst will be harder, thereby reducing the quantity and quality of biofuels. The use of Ni(A)-NH_2/LM catalyst three times without a regeneration process was able to maintain the quantity of biofuel at around 80 wt.%, whereas the hydrocarbon level showed a decrease, but not less than 45% of the liquid product (wt.%). This is very reasonable because it is related to the formation of coke which leads to the deactivation of the catalyst. Overall, these results suggest good catalytic performance may offer an alternative pathway for the production of more environmentally friendly fuels in the future.

■ ACKNOWLEDGMENTS

The authors would like to thank the Ministry of Research, Technology, and Higher Education of Indonesia for the financial support under the scheme of PTUPT research grant 2021 (Contract Number: 2127/UN1/DITLIT/DIT-LIT/PT/2021) and also the Faculty of Mathematics and Natural Sciences, Universitas Gadjah Mada for the additional financial support under *Hibah Penelitian Dosen* 2021 (Contract Number: 148/J01.1.28/PL.06.02/2021).

■ REFERENCES

[1] Kusumastuti, H., Trisunaryanti, W., Falah, I.I., and Marsuki, M.F., 2018, Synthesis of mesoporous silica-alumina from lapindo mud as a support of Ni and Mo metals catalysts for hydrocracking of pyrolyzed α-cellulose, *Rasayan J. Chem.*, 11 (2), 522–530.

[2] Vazquez, N.I., Gonzalez, Z., Ferrari, B., and Castro, Y., 2017, Synthesis of mesoporous silica nanoparticles by sol-gel as nanocontainer for future drug delivery applications, *Bol. Soc. Esp. Ceram. Vidrio*, 56 (3), 139–145.

[3] Niculescu, V.C., 2020, Mesoporous silica nanoparticles for bio-applications, *Front. Mater.*, 7, 36.

[4] Rizzi, F., Castaldo, R., Latronico, T., Lasala, P., Gentile, G., Lavorgna, M., Striccoli, M., Agostiano, A., Comparelli, R., Depalo, N., Curri, M.L., and Fanizza, E., 2021, High surface area mesoporous silica nanoparticles with tunable size in the sub-micrometer regime: Insights on the size and porosity control mechanisms, *Molecules*, 26 (14), 4247.

[5] Lin, Y.S., Hurley, K.R., and Haynes, C.L., 2012, Critical considerations in the biomedical use of mesoporous silica nanoparticles, *J. Phys. Chem. Lett.*, 3 (3), 364–374.)

[6] Kumar, S., Malik, M.M., and Purohit, R., 2017, Synthesis methods of mesoporous silica materials, *Mater. Today: Proc.*, 4 (2), 350–357.

[7] Trisunaryanti, W., Larasati, S., Bahri, S., Ni'mah, Y.L., Efiyanti, L., Amri, K., Nuryanto, R., and

Sumbogo, S.D., 2020, Performance comparison of Ni-Fe loaded on NH_2-functionalized mesoporous silica and beach sand in the hydrotreatment of waste palm cooking oil, *J. Environ. Chem. Eng.*, 8 (6), 104477.

[8] Trisunaryanti, W., Triyono, Paramesti, C., Larasati, S., Santoso, N.R., and Fatmawati, D.A., 2020, Synthesis and characterization of Ni-NH_2/mesoporous silica catalyst from Lapindo mud for hydrocracking of waste cooking oil into biofuel, *Rasayan J. Chem.*, 13, 1386–1393.

[9] Li, G., Chen, L., Fan, R., Liu, D., Chen, S., Li, X., and Chung, K.H., 2019, Catalytic deoxygenation of C 18 fatty acid over supported metal Ni catalysts promoted by the basic sites of $ZnAl_2O_4$ spinel phase, *Catal. Sci. Technol.*, 9 (1), 213–222.

[10] Jang, M.S., Phan, T.N., Chung, I.S., Lee, I.G., Park, Y.K., and Ko, C.H., 2018, Metallic nickel supported on mesoporous silica as catalyst for hydrodeoxygenation: Effect of pore size and structure, *Res. Chem. Intermed.*, 44 (6), 3723–3735.

[11] Paramesti, C., Trisunaryanti, W., Sudiono, S., Triyono, T., Larasati, S., Santoso, N.R., and Fatmawati, D.A., 2021, The influence of metal loading amount on Ni/mesoporous silica extracted from Lapindo mud templated by CTAB for conversion of waste cooking oil into biofuel, *Bull. Chem. React. Eng. Catal.*, 16 (1), 22–30.

[12] Lu, H.T., 2013, Synthesis and characterization of amino-functionalized silica nanoparticles, *Colloid J.*, 75 (3), 311–318.

[13] Ma, Y., Wu, Y., Lee, J.G., He, L., Rother, G., Fameau, A.L., Shelton, W.A., and Bharti, B., 2020, Adsorption of fatty acid molecules on amine-functionalized silica nanoparticles: Surface organization and foam stability, *Langmuir*, 36 (14), 3703–3712.

[14] Kandel, K., Frederickson, C., Smith, E.A., Lee, Y.J., and Slowing, I.I., 2013, Bifunctional adsorbent-catalytic nanoparticles for the refining of renewable feedstocks, *ACS Catal.*, 3, 2750–2758.

[15] Chuah, L.F., Mohd Salleh, N.H., Osnin, N.A., Alcaide, J.I., Abdul Majid, M.H., Abdullah, A.A., Bokhari, A., A Jalil, E.E., and Klemeš, J.J., 2021, Profiling Malaysian ship registration and seafarers for streamlining future Malaysian shipping governance, *Aust. J. Marit. Ocean Aff.*, 13 (4), 225–261.

[16] Nanda, S., Rana, R., Hunter, H.N., Fang, Z., Dalai, A.K., and Kozinski, J.A., 2019, Hydrothermal catalytic processing of waste cooking oil for hydrogen-rich syngas production, *Chem. Eng. Sci.*, 195, 935–945.

[17] Ong, A.S.H., and Goh, S.H., 2002, Palm oil: A healthful and cost-effective dietary component, *Food Nutr. Bull.*, 23 (1), 11–22.

[18] Hartono, Z.A., and Cahyono, B., 2020, Effect of using B30 palm oil biodiesel to deposit forming and wear metal of diesel engine components, *Int. J. Mar. Eng. Innovation Res.*, 5 (1), 10–19.

[19] Ayetor, G.K., Sunnu, A., and Parbey, J., 2015, Effect of biodiesel production parameters on viscosity and yield of methyl esters: *Jatropha curcas*, *Elaeis guineensis* and *Cocos nucifera*, *Alexandria Eng. J.*, 54, 1285–1290.

[20] Goswami, G., Bora, R., and Rathore, M.S., 2016, Oxidation of cooking oils due to repeated frying and human health, *Int. J. Sci. Technol. Manage.*, 4 (1), 495–501.

[21] Huang, D., Zhou, H., and Lin, L., 2012, Biodiesel: An alternative to conventional fuel, *Energy Procedia*, 16, 1874–1885.

[22] Murachman, B., Deendarlianto, D., Nissaraly, H.F., and Hasyim, W., 2014, Experimental study on hydrocracking process of asbuton hydrocarbon based on the aromatic, and waxy residue based on paraffinic, by using Pt/Pd and γ-alumina catalyst in a fixed bed reactor, *ASEAN J. Chem. Eng.*, 14 (1), 59–75.

[23] Treese, S.A., Pujadó, P.R., and Jones, D.S.J., 2015, *Handbook of Petroleum Processing*, Springer, Cham, Switzerland.

[24] Alkhaldi, S., and Husein, M.M., 2014, Hydrocracking of heavy oil by means of in situ prepared ultradispersed nickel nanocatalyst, *Energy Fuels*, 28 (1), 643–649.

[25] Khoiri, H.M., Trisunaryanti, W., and Dewi, K., 2015, Synthesis of NH_2/MCM-41 catalysts using

silica of Sidoarjo mud and their characterization for palm oil transesterification, *IOSR J. Appl. Chem.*, 8 (8), 50–56.

[26] Nugrahaningtyas, K.D., Trisunaryanti, W., Triyono, T., Nuryono, N., Widjonarko, D.M., Yusnani, A., and Mulyani, M., 2009, Preparation and characterization the non-sulfided metal catalyst: Ni/USY and NiMo/USY, *Indones. J. Chem*., 9 (2), 177–183.

[27] Kefaifi, A., Sahraoui, T., Kheloufi, A., and Drouiche, N., 2018, Silica sand etching behavior during leaching process using design of experiments method (DOE), *Silicon*, 10 (3), 1187–1193.

[28] Dubey, R.S., Rajesh, Y.B.R.D., and More, M.A., 2015, Synthesis and characterization of SiO_2 nanoparticles via sol-gel method for industrial applications, *Mater. Today: Proc.*, 2 (4-5), 3575–3579.

[29] Li, X., Han, C., Zhu, W., Ma, W., Luo, Y., Zhou, Y., Yu, J., and Wei, K., 2014, Cr(VI) removal from aqueous by adsorption on amine-functionalized mesoporous silica prepared from silica fume, *J. Chem.*, 2014, 765856.

[30] Oliveira, D.M., and Andrada, A.S., 2019, Synthesis of ordered mesoporous silica MCM-41 with controlled morphology for potential application in controlled drug delivery systems, *Cerâmica*, 65, 170–179.

[31] Cychosz, K.A., and Thommes, M., 2018, Progress in the physisorption characterization of nanoporous gas storage materials, *Engineering*, 4 (4), 559–566.

[32] Thommes, M., Kaneko, K., Neimark, A.V., Olivier, J.P., Rodriguez-Reinoso, F., Rouquerol, J., and Sing, K.S.W., 2015, Physisorption of gases, with special reference to the evaluation of surface area and pore size distribution (IUPAC Technical Report), *Pure Appl. Chem.*, 87 (9-10), 1051–1069.

[33] Trisunaryanti, W., Wijaya, K., Triyono, T., Adriani, A.R., and Larasati, S., 2021, Green synthesis of hierarchical porous carbon prepared from coconut lumber sawdust as Ni-based catalyst support for hydrotreating Callophyllum inophyllum oil, *Results Eng.*, 11, 100258.

[34] Qi, L., Tang, X., Wang, Z., and Peng, X., 2017, Pore characterization of different types of coal from coal and gas outburst disaster sites using low temperature nitrogen adsorption approach, *Int. J. Min. Sci. Technol.*, 27 (2), 371–377.

[35] Junaidi, R., Hasan, A., and Zamhari, M., 2019, Influence the addition of Lapindo mud is calcined to the quality of cement podzoland by using electric furnace, *J. Phys.: Conf. Ser.*, 1167, 012043.

[36] Hu, H., Lu, S., Li, T., Zhang, Y., Guo, C., Zhu, H., Jin, Y., Du, M., and Zhang, W., 2021, Controlled growth of ultrafine metal nanoparticles mediated by solid supports, *Nanoscale Adv*., 3 (7), 1865–1886.

[37] Ochoa-Hernández, C., Yang, Y., Pizarro, P., de La Peña O'Shea, V.A., Coronado, J.M., and Serrano, D.P., 2013, Hydrocarbons production through hydrotreating of methyl esters over Ni and Co supported on SBA-15 and Al-SBA-15, *Catal. Today*, 210, 81–88.

[38] Auepattana-aumrung, C., Márquez, V., Wannakao, S., Jongsomjit, B., Panpranot, J., and Praserthdam, P., 2020, Role of Al in Na-ZSM-5 zeolite structure on catalyst stability in butene cracking reaction, *Sci. Rep.*, 10 (1), 13643.

[39] Anderson, J.E., Dicicco, D.M., Ginder, J.M., Kramer, U., Leone, T.G., Raney-Pablo, H.E., and Wallington, T.J., 2012, High octane number ethanol-gasoline blends: Quantifying the potential benefits in the United States, *Fuel*, 97, 585–594.

[40] Kubička, D., and Kaluža, L., 2010, Deoxygenation of vegetable oils over sulfided Ni, Mo and NiMo catalysts, *Appl. Catal., A*, 372 (2), 199–208.